*J Mater Sci: Mater Electron* **(2024) 35:409**

# Influence of ionizing radiation on admittance measurements of $Au/TiO_2$/n-Si (MIS) capacitor

Mehmet İzdeş[1], Raziye Ertuğrul Uyar[1,*], and Adem Tataroğlu[1]

[1] *Department of Physics, Faculty of Sciences, Gazi University, Ankara 06500, Turkey*


**Received:** 5 December 2023
**Accepted:** 13 February 2024
**Published online:**
26 February 2024

© The Author(s), 2024


## ABSTRACT

This study aimed to investigate the influence of ionizing radiation on the admittance measurements of Titanium dioxide ($TiO_2$)-based metal-insulator-semiconductor (MIS) capacitor. The capacitor was irradiated to a cumulative dose of 100 kGy using a $^{60}$Co-gamma (γ) source. The electrical admittance ($Y = G + i\omega C$) measurements of the MIS capacitor were performed before and after exposure to gamma irradiation for four different frequencies (1, 10, 100 and 500 kHz). Gamma irradiation leads to changes in the capacitance/conductance versus voltage (C/G–V) characteristics. The C and G showed a decrease by increasing the radiation dose and frequency. This decrease is attributed to the interface traps and oxide-trapped charges created during the gamma irradiation. The obtained results showed that the prepared MIS capacitor have great potential for dosimetry applications.


## 1 Introduction

Electronic and optoelectronic devices such as diodes, metal-insulator/oxide-semiconductor (MIS-MOS) field-effect transistors, sensors, capacitors, and junction field-effect phototransistors are much more sensitive to ionizing radiation. The electrical and dielectric parameters including capacitance, conductivity, dielectric constant and dielectric loss tangent of these devices show sensitivity to radiation. The most sensitive part to radiation in these devices is the semiconductor and oxide/insulator layer. Dielectric or insulating materials are second to semiconductor devices in terms of sensitivity to radiation. Ionizing radiation can induce significant charge buildup in oxides. This may lead to degradation or even complete failure of devices. The gate oxide layers are commonly used in MOS-based devices such as radiation sensors, dosimeters and transistors. On the other hand, when a semiconductor device is exposed to high-energy ionizing irradiation, charge carriers generated by radiation in the semiconductor are carried by diffusion-drift. These carriers do not affect the electronic parameters of the devices. At the same time, electron-hole pairs generated by ionizing radiation in oxide layer induce the buildup of charge. The radiation-induced charge buildup can lead to device degradation and circuit failure [1–7].

Ionizing radiation sources such as high-energy photons (gamma and X-rays) or neutrons, beta particles, protons, and alpha particles are used to investigate radiation effects in electronic applications. Gamma radiation, which penetrates and interacts with matter,

Address correspondence to E-mail: raziyeertugrul@hotmail.com

https://doi.org/10.1007/s10854-024-12189-0

is one of the major radiation sources. There are three mechanisms of gamma radiation interaction with matter: (1) pair production (2) Compton scattering, and (3) photoelectric effect. Some radionuclides that emit gamma rays are cobalt-60, caesium-137, iridium-192 and technetium-99 m.

Titanium oxide ($TiO_2$) is one of the important transition metal oxides. It has unique properties such as high chemical and thermal stability, refractive index, dielectric constant and low absorption [8–11]. $TiO_2$ is also a wide band-gap semiconductor. $TiO_2$ is widely used in various semiconductor device applications such as transistors, capacitors, solar cells, batteries, and sensors. The most commonly used methods to deposit $TiO_2$ thin film on a substrate are the RF-magnetron sputtering, chemical vapor deposition, and sol-gel.

In the previous article, we studied the effect of radiation on current–voltage (I–V) characteristics of the Au-/$TiO_2$/-n-Si (MIS) capacitor [11]. In the present work, we examined the effects of gamma-ray irradiation on the C–G–V characteristics of the MIS capacitor with $TiO_2$ dielectric for irradiation doses from 5 to 100 kGy.

## 2 Experimental details

The formation of the titanium dioxide ($TiO_2$) as an interlayer film and the fabrication process of Au/$TiO_2$/n-Si (MIS) structure was given in detail in our previous study [11]. HP 4192 A LF Impedance Analyzer (5 Hz–13 MHz) was used to measure the admittance ($Y = G + i\omega C$) of the MIS device. The MIS-capacitor was irradiated with $^{60}$Co-gamma ($\gamma$)-ray source at a dose rate of 0.69 kGy/h and was exposed to different radiation doses (5, 10, 50 and 100 kGy).

## 3 Results and discussion

Electrical admittance ($Y = G + i\omega C$) or impedance ($Z = 1/Y$) spectroscopy is a simple and fast technique for characterizing of electronic devices. The Au/$TiO_2$/n-Si (MIS) capacitor was subjected to different dose of irradiation. The capacitance and conductance of the capacitor was measured using the impedance analyzer before and after the irradiation process. Figures 1a–d and 2a–d demonstrate the C–V and G/ω–V measurements of MIS capacitor for 1 kHz, 10 kHz, 100 kHz, and 500 kHz frequencies before and after irradiation, respectively. These measurements showed that radiation had a significant impact on the MIS capacitor. In other words, gamma radiation leads to defect generation in the MIS capacitor. As seen in these figures, as the irradiation dose increases, the capacitance and conductance decrease. This decrease indicates that oxide-trapped charges and interface traps in the $TiO_2$ and $TiO_2$/Si interface are created during the gamma irradiation [1, 2, 12–18]. When an MOS capacitor is exposed to ionizing irradiation, electron-hole pairs are produced in oxide layer. The free charge carriers cause the buildup of charges. This may cause to device degradation and therefore circuit failure. Besides, the C–V plots for each irradiation dose exhibit a peak occurring in in depletion region. This peak is due to the change of interface trap charges due to the radiation response of the MIS capacitor. The interface traps/surface states ($N_{ss}$) are generally effective in the depletion region at low and intermediate frequencies. However, the peak behavior observed in the accumulation region at enough high frequencies results from the presence of series resistance ($R_s$).

Moreover, as seen in these figures, a tendency to decrease in capacitance and conductance was observed as the frequency increased. This frequency-dependent state is due to the presence of interface states in $TiO_2$/Si interface [3, 19, 20]. The magnitude of the capacitance is determined by the ability to follow the frequency of the interface states. At the high frequencies, the carrier lifetime ($T = 1/\omega$) in interface charge traps is greater than $1/2\pi f$. In this case, the interface states cannot adequately follow applied ac signal and so they do not contribute to capacitance [21–26]. Therefore, the capacitance value is low compared to low frequencies.

Additionally, the C–V curves plotted at 500 kHz exhibit an anomalous peak for each radiation dose in the forward-bias due to the interfacial polarization, series resistance and interface traps, and then the C values becomes negative. The abnormal case is known as negative capacitance (NC) behavior. NC occurs due to the fact that an increase in the applied bias voltage causes a decrease in the number of charges on the electrodes [27–31]. NC also indicates that the device exhibits an inductive behavior.

One of the parameters affecting the performance of the semiconductor devices is series resistance ($R_s$), which is effective only in the accumulation region. The $R_s$ value of the MIS capacitor was calculated using

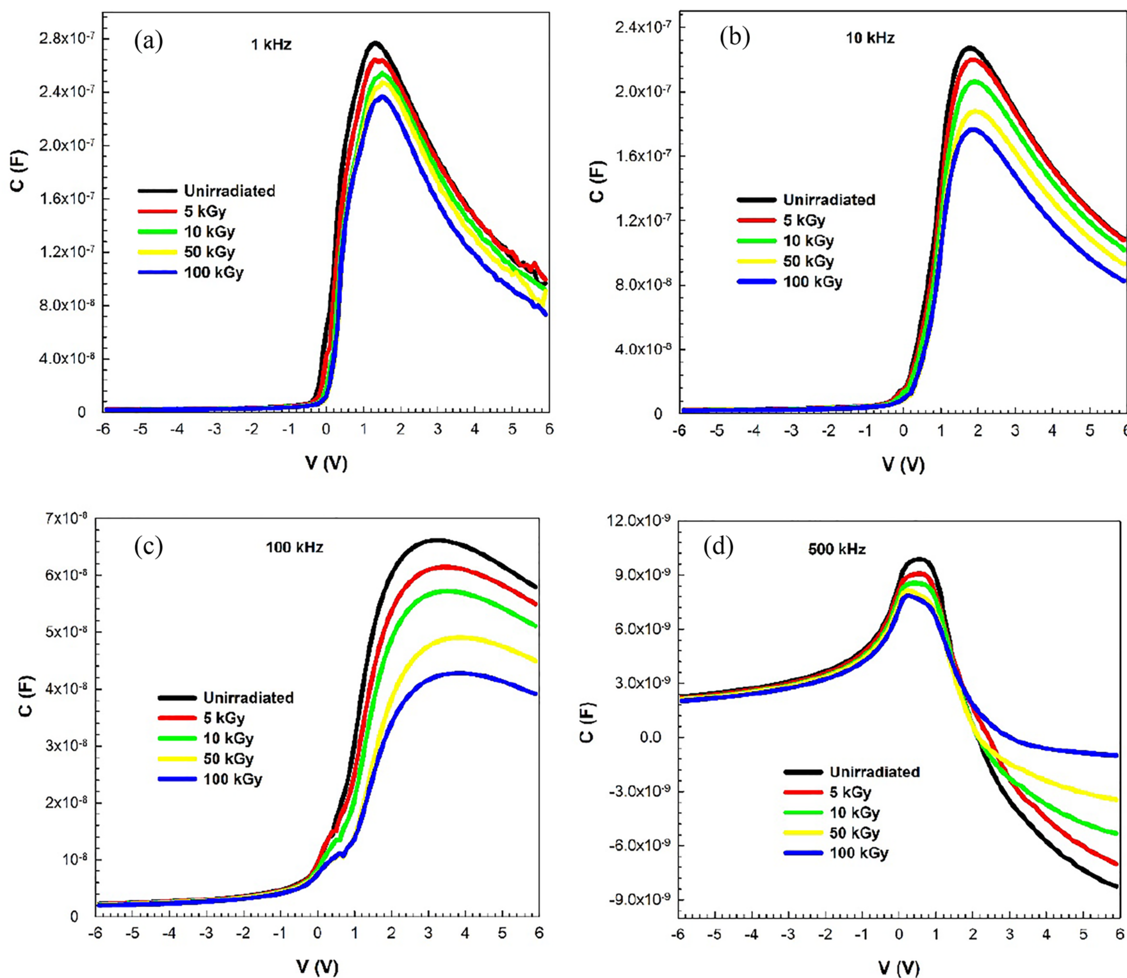


**Fig. 1** C–V plots of the MIS before and after irradiation at various frequencies: **a** 1 kHz, **b** 10 kHz, **c** 100 kHz, **d** 500 kHz

the measured C and G data at a strong accumulation region in the equation given below [3, 32].

$$R_s = \frac{G_m}{G_m^2 + (\omega C_m)^2} \quad (1)$$

The $R_s$–V plots of the MIS capacitor for 1 kHz, 10 kHz, 100 and 500 kHz frequencies before and after gamma irradiation are presented in Fig. 3a–d, respectively. As seen in these figures, it was observed that the $R_s$ value for each frequency increased as the radiation dose increased. This increase is due to the effect of displacement damage caused by ionizing radiation as well as the reduction of free carrier density with irradiation [33–35]. Besides, defects induced by gamma-irradiation result in decreased carrier mobility. This leads to the increase the device resistance. In addition, the $R_s$–V plots showed a peak in the depletion region. This peak comes from the existence of interface trapped charges.

Additionally, in order to extract the other electronic parameters of the prepared MIS capacitor including the intercept-voltage/built-in potential ($V_0$), concentration of donor atoms ($N_D$), Fermi-energy ($E_F$), barrier height ($\Phi_B$), and depletion layer width ($W_D$), $1/C^2$–V plot is drawn and this plot should give a straight line or linear region due to the space charge becoming uniform throughout depletion layer. These parameters are determined from the slope and intercept of the linear region of this plot.

The relation between depletion layer capacitance and voltage is given by Refs. [3, 36–43]. ,

$$\frac{1}{C^2} = \frac{2(V_0 + V)}{\epsilon_s \epsilon_0 e A^2 N_D}, \quad (2)$$

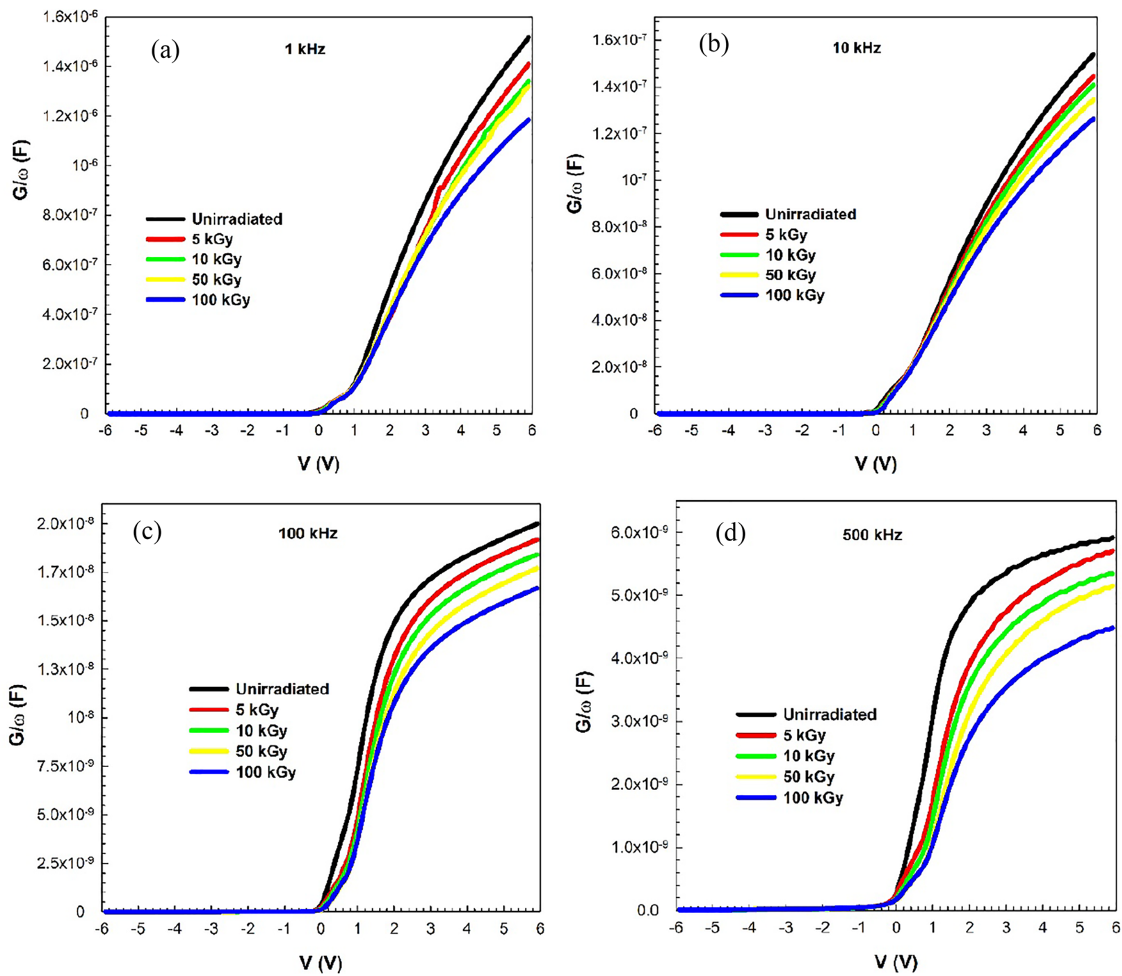


**Fig. 2** G/ω–V curves **a** 1 kHz, **b** 10 kHz, **c** 100 kHz, **d** 500 kHz

where e is electronic charge, A is the area of device, V is the applied bias, $\varepsilon_s$ (= 11.9) is a dielectric constant of Si and $\varepsilon_0$ (= $8.85 \times 10^{14}$ F/cm) is the vacuum permittivity. The value of $V_0$ and $N_D$ are computed from the intercept and slope of straight line of $1/C^2$–V curve, respectively. The magnitude of diffusion-potential ($V_D$), the maximum electrical field ($E_m$), the image-force barrier lowering ($\Delta\Phi_B$), $E_F$, and $W_D$ using the calculated $V_0$ and $N_D$ data, were obtained from the next equations,

From here, the $\Phi_B$ can be expressed as follows,

$$\varnothing_B = V_D + \frac{kT}{e}\ln\left(\frac{N_C}{N_D}\right) - \Delta\varnothing_B = V_D + E_F - \Delta\varnothing_B \quad (4)$$

Barrier height is inversely proportional to donor concentration.

Figure 4 a–d shows the $C^2$–V plots of the MIS capacitor for four frequencies, i.e., 1 kHz, 10 kHz, 100 and 500 kHz before and after gamma irradiation.

$$V_D = V_0 + \frac{kT}{e}, \quad E_F = \frac{kT}{e}\text{In}\left(\frac{N_C}{N_D}\right), \quad E_m = \left[\frac{2eN_DV_0}{\epsilon_s\epsilon_0}\right]^{0.5}, \quad \delta\varnothing_b = \left[\frac{eE_m}{4\pi\epsilon_s\epsilon_0}\right]^{0.5}, \quad W_D = \sqrt{\frac{2\epsilon_s\epsilon_0V_D}{eN_D}} \quad (3)$$

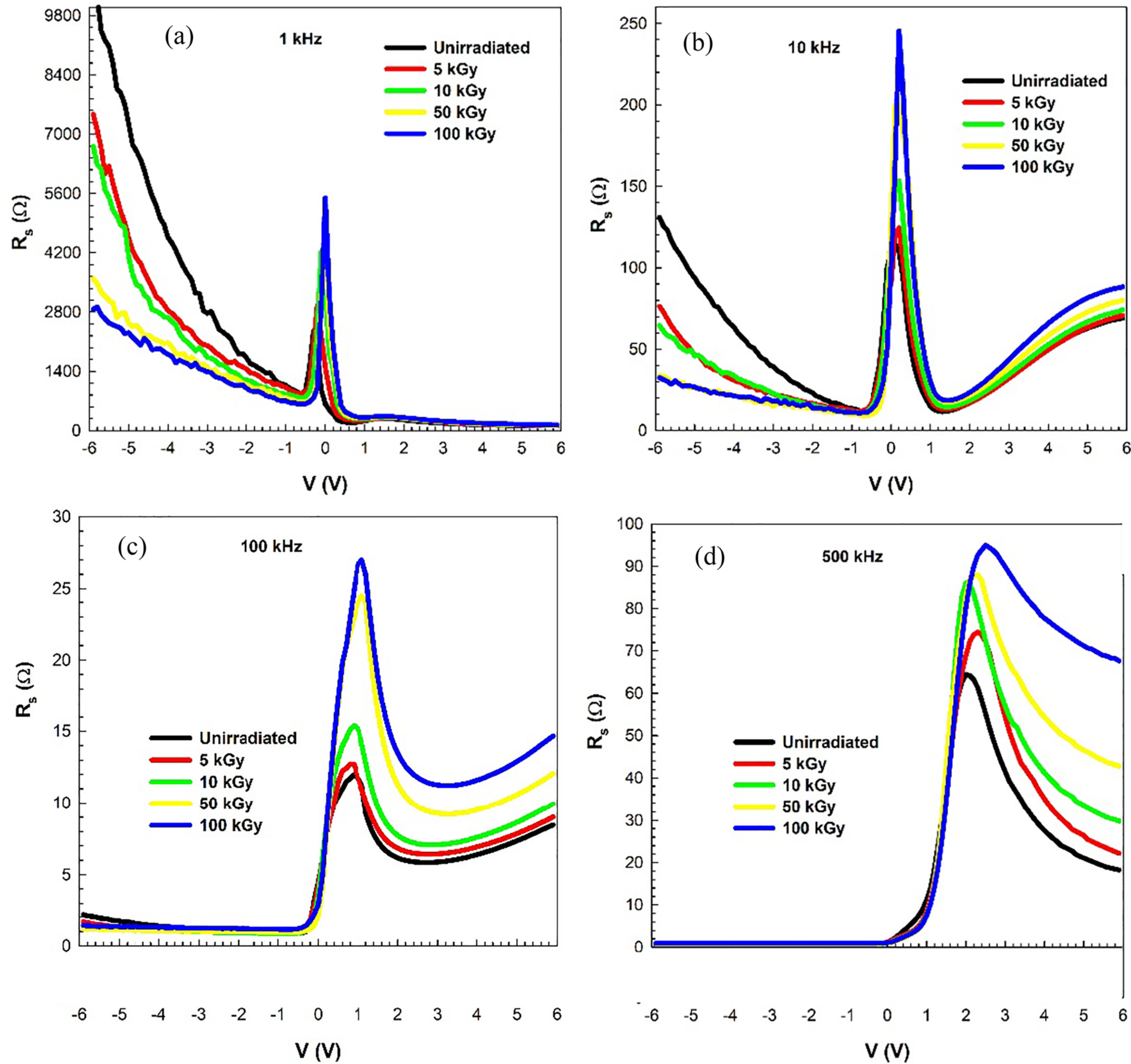


**Fig. 3** $R_s$–V plots **a** 1 kHz, **b** 10 kHz, **c** 100 kHz, **d** 500 kHz

For all frequencies, it is seen that these plots indicate a linear plot characteristic in the reverse-bias region and wide voltage range. All electronic parameters are obtained from the slope and intercept of the linear part.

The values of calculation parameters such as $V_0$, $V_D$, $N_D$, $E_F$, $\Delta\Phi_B$, $\Phi_B$ and $W_D$ are listed in Tables 1, 2, 3 and 4, respectively. It is observed that these parameters strongly depend on both frequency and irradiation dose. For all frequencies, as the radiation dose increases, $V_0$, $V_D$, $\Phi_B$ and $W_D$ values increase, while $N_D$ value decreases. The gamma irradiation causes an increase in the barrier height and diffusion-potential. The increase in $\Phi_B$ and $V_D$ can also be explained by the emergence of radiation-induced interface defects at the interface [36–38]. Also, the decrease of $N_D$ with irradiation can be cause to the gamma irradiation-induced lattice defects, traps, and vacancies. Irradiation can induce defects in the bulk as well as in the interlayer film. The defects may cause changes in electrical properties of device and may damage device performance. In addition, as the frequency increases, $N_D$ and $\Phi_B$ value increase. This increase is due to the change of interface states that cannot enough follow the ac signal at high-frequencies [44–46].

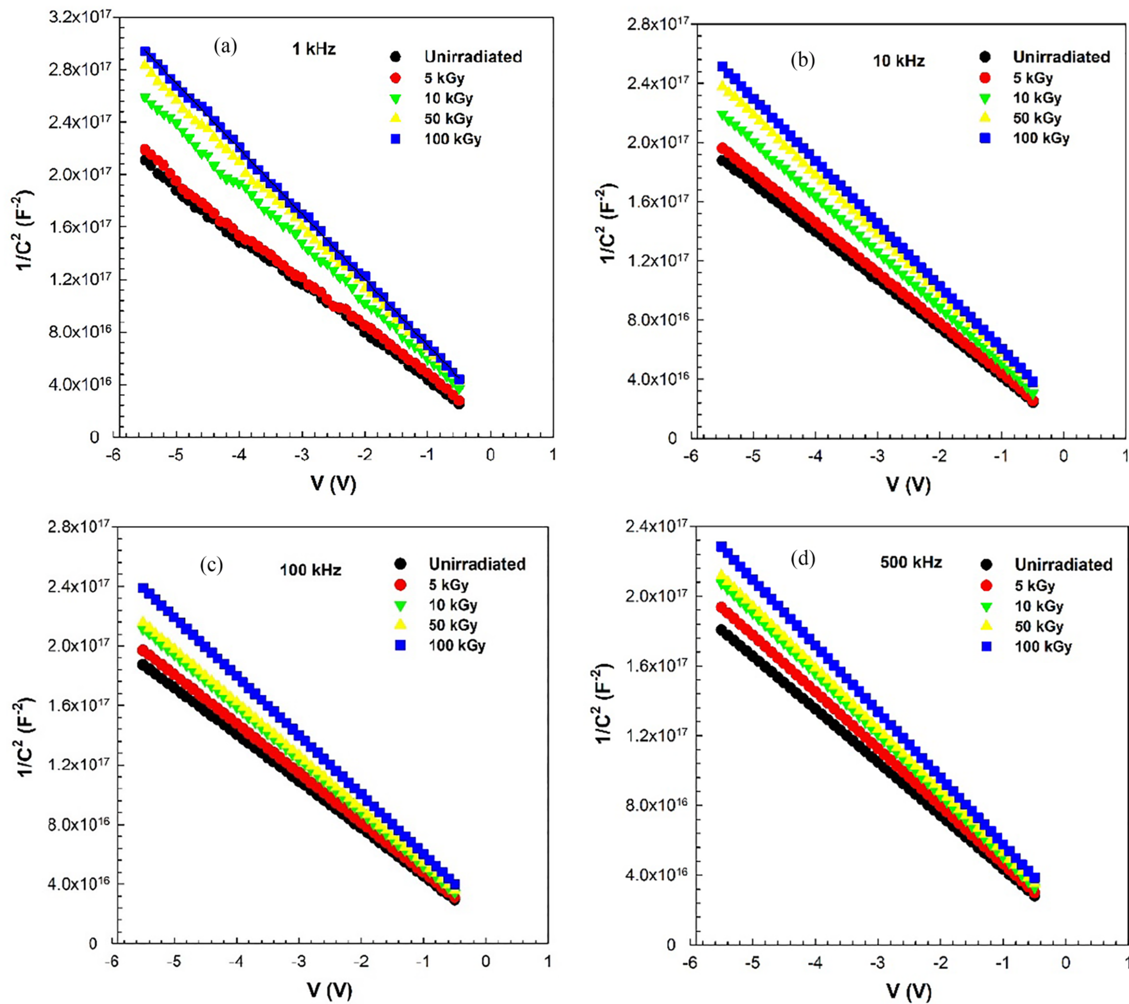


**Fig. 4** $1/C^2$ versus V plots: **a** 1 kHz, **b** 10 kHz, **c** 100 kHz, **d** 500 kHz

**Table 1** Electrical parameters calculated from $1/C^2$–V characteristics for 1 kHz at different irradiation doses

| Irrad. dose (kGy) | $V_0$ (V) | $V_D$ (eV) | $N_D \times 10^{17}$ ($cm^{-3}$) | $E_F$ (eV) | $\Delta\Phi_B$ (eV) | $\Phi_B$ (eV) | $W_D \times 10^{-6}$ (cm) |
|---|---|---|---|---|---|---|---|
| 0 | 0.217 | 0.242 | 3.335 | 0.115 | 0.044 | 0.314 | 3.094 |
| 5 | 0.288 | 0.314 | 3.276 | 0.115 | 0.046 | 0.383 | 3.551 |
| 10 | 0.349 | 0.375 | 2.725 | 0.120 | 0.046 | 0.449 | 4.256 |
| 50 | 0.395 | 0.421 | 2.535 | 0.122 | 0.047 | 0.496 | 4.673 |
| 100 | 0.406 | 0.432 | 2.415 | 0.123 | 0.046 | 0.509 | 4.854 |

## 4 Conclusions

In this experimental study, we report the influence of ionizing radiation on admittance measurements of Au/$TiO_2$/n-Si (MIS) capacitor. The MIS capacitor in different radiation doses up to 100 kGy and a wide range of frequencies between 1 and 500 kHz were studied. The experimental results demonstrate that the capacitance and conductance of the MIS capacitor exhibited a linear decrease by increasing the radiation dose and frequencies. This decrease is attributed

**Table 2** Electrical parameters for 10 kHz

| Irrad. dose (kGy) | $V_0$ (V) | $V_D$ (eV) | $N_D \times 10^{17}$ ($cm^{-3}$) | $E_F$ (eV) | $\Delta\Phi_B$ (eV) | $\Phi_B$ (eV) | $W_D \times 10^{-6}$ (cm) |
|---|---|---|---|---|---|---|---|
| 0 | 0.276 | 0.302 | 3.685 | 0.112 | 0.047 | 0.367 | 3.286 |
| 5 | 0.298 | 0.324 | 3.549 | 0.113 | 0.048 | 0.389 | 3.467 |
| 10 | 0.356 | 0.382 | 3.210 | 0.116 | 0.048 | 0.449 | 3.956 |
| 50 | 0.427 | 0.453 | 2.994 | 0.117 | 0.050 | 0.521 | 4.463 |
| 100 | 0.432 | 0.458 | 2.842 | 0.119 | 0.049 | 0.528 | 4.606 |

**Table 3** Electrical parameters for 100 kHz

| Irrad. dose (kGy) | $V_0$ (V) | $V_D$ (eV) | $N_D \times 10^{17}$ ($cm^{-3}$) | $E_F$ (eV) | $\Delta\Phi_B$ (eV) | $\Phi_B$ (eV) | $W_D \times 10^{-6}$ (cm) |
|---|---|---|---|---|---|---|---|
| 0 | 0.448 | 0.474 | 3.809 | 0.111 | 0.053 | 0.532 | 4.047 |
| 5 | 0.449 | 0.474 | 3.624 | 0.112 | 0.053 | 0.534 | 4.152 |
| 10 | 0.473 | 0.499 | 3.391 | 0.114 | 0.052 | 0.561 | 4.402 |
| 50 | 0.516 | 0.542 | 3.354 | 0.114 | 0.053 | 0.603 | 4.611 |
| 100 | 0.516 | 0.542 | 3.026 | 0.117 | 0.052 | 0.607 | 4.855 |

**Table 4** Electrical parameters for 500 kHz

| Irrad. dose (kGy) | $V_0$ (V) | $V_D$ (eV) | $N_D \times 10^{17}$ ($cm^{-3}$) | $E_F$ (eV) | $\Delta\Phi_B$ (eV) | $\Phi_B$ (eV) | $W_D \times 10^{-6}$ (cm) |
|---|---|---|---|---|---|---|---|
| 0 | 0.429 | 0.455 | 3.948 | 0.110 | 0.053 | 0.512 | 3.896 |
| 5 | 0.434 | 0.460 | 3.676 | 0.112 | 0.052 | 0.520 | 4.060 |
| 10 | 0.451 | 0.477 | 3.446 | 0.114 | 0.052 | 0.539 | 4.268 |
| 50 | 0.501 | 0.526 | 3.408 | 0.114 | 0.053 | 0.587 | 4.510 |
| 100 | 0.519 | 0.545 | 3.168 | 0.116 | 0.053 | 0.609 | 4.760 |

to the interface traps and oxide-trapped charges created during the gamma irradiation. Results of the study, it was observed that the $R_s$ value for each frequency increased as the radiation dose increased. This increase is due to the effect of displacement damage caused by ionizing radiation as well as the reduction of free carriers with irradiation. Based on the results, it can be concluded that the prepared MIS capacitor have immense potential for used as solid state radiation detector.

## Author contributions

The manuscript was written with the contributions of all authors. All authors have approved the final version of the manuscript. Mİ: Investigation, measurements, writing, review and editing. REU: Investigation, measurements, writing, review and editing. AT: Investigation, writing, review and editing, supervision.

## Funding

Open access funding provided by the Scientific and Technological Research Council of Türkiye (TÜBİTAK). The authors declare that no funds, grants, or other support were received during the preparation of this manuscript.

## Data availability

The datasets generated during and/or analyzed during the current study are available from the corresponding author on reasonable request.

## Declarations

**Conflict of interest** There are no conflicts to declare.

**Open Access** This article is licensed under a Creative Commons Attribution 4.0 International License, which permits use, sharing, adaptation, distribution and reproduction in any medium or format, as long as you give appropriate credit to the original author(s) and the source, provide a link to the Creative Commons licence, and indicate if changes were made. The images or other third party material in this article are included in the article's Creative Commons licence, unless indicated otherwise in a credit line to the material. If material is not included in the article's Creative Commons licence and your intended use is not permitted by statutory regulation or exceeds the permitted use, you will need to obtain permission directly from the copyright holder. To view a copy of this licence, visit http://creativecommons.org/licenses/by/4.0/.

## References

1. T.P. Ma, P.V. Dressendorfer, *Ionizing Radiation Effects in MOS Devices and Circuits* (Wiley, New York, 1989)
2. T.R. Oldham, *Ionizing Radiation Effects in MOS Oxides* (World Scientific, Singapore, 1999)
3. E.H. Nicollian, J.R. Brews, *MOS Physics and Technology* (Wiley, New York, 1982)
4. M. Bagatin, S. Gerardin, *Ionizing Radiation Effects in Electronics: From Memories to Imagers* (CRC, Boca Raton, 2016)
5. H.L. Olesen, *Radiation Effects on Electronic Systems* (Plenum, New York, 1966)
6. L. Junxing, L. Changshi, Radiat. Phys. Chem. **212**, 111165 (2023)
7. A. Tataroglu, J. Mater. Electron. Device. **1**, 6–10 (2017)
8. F. Parrino, L. Palmisano, *Titanium Dioxide ($TiO_2$) and Its Applications* (Elsevier, Amsterdam, 2020)
9. B.R. Weinberger, R.B. Garber, Appl. Phys. Lett. **66**, 2409–2411 (1995)
10. S.C. Shei, Ann. Mater. Sci. Eng. **2013**, 545076 (2013)
11. R. Ertugrul-Uyar, A. Buyukbas-Ulusan, A. Tataroglu, J. Mater. Sci. Mater. Electron. **31**, 19846–19851 (2020)
12. A. Tataroğlu, M. Yıldırım, H.M. Baran, Mater. Sci. Semicond. Proc. **28**, 89–93 (2014)
13. Y. Lia, Y. Ma, W. Lin, P. Dong, Z. Yang, M. Gong, J. Bi, B. Li, K. Xi, G. Xu, Superlattices Microstruct. **120**, 313–318 (2018)
14. V. Kumar, S. Kumar, A.S. Maan, J. Akhtar, Appl. Nanosci. **13**, 3181–3188 (2023)
15. E. Efil Kutluoglu, E. Oz Orhan, O. Bayram, S. Bilge Ocak, Physica B **621**, 413306 (2021)
16. R. Ertuğrul, A. Tataroğlu, Radiat. Eff. Defects Solids. **169**, 791–799 (2014)
17. M.R. Shaneyfelt, IEEE Trans. Nucl. Sci. **49**, 3191–3196 (2002). J.G. Hong, G. Lucovsky, J.R. Schwank
18. A. Kahraman, A. Mutale, R. Lok, E. Yilmaz, Radiat. Phys. Chem. **196**, 110138 (2022)
19. D.K. Schroder, *Semiconductor Material and Device Characterization*, 2nd edn. (Wiley, New York, 1998)
20. H. Bentarzi, *Transport in Metal-Oxide-Semiconductor Structures* (Springer, New York, 2011)
21. F.Z. Acar, A. Buyukbas–Ulusan, A. Tataroglu, J. Mater. Sci. Mater. Electron. **29**, 12553–12560 (2018)
22. S. Alptekin, A. Tataroğlu, Ş. Altındal, J. Mater. Sci. Mater. Electron. **30**, 6853–6859 (2019)
23. Ö. Berkün, M. Ulusoy, Ş. Altındal, B. Avar, Physica B **666**, 415099 (2023)
24. D.E. Yıldız, A. Tataroglu, J. Mater. Sci. Mater. Electron. **34**, 1057 (2023)
25. P.N. Meitei, N. Khelchand Singh, J. Alloys Compd. **941**, 168900 (2023)
26. A. Cherif, S. Alotaibi, H. Saghrouni, L. Beji, AIP Adv. **13**, 025042 (2023)
27. B.K. Jones, J. Santana, M. McPherson, Solid State Commun. **107**, 47–50 (1998)
28. E.E. Tanrıkulu, S. Demirezen, Ş Altındal, İ Uslu, J. Mater. Sci. Mater. Electron. **29**, 2890–2898 (2018)
29. J.-G. Ma, K.S. Yeo, M.A. Do, IEEE Trans. Electron. Devices. **46**, 2357–2358 (1999)
30. N. Delen, S. Altındal Yeriskin, A. Ozbay, I. Tascıoglu, Physica B **665**, 415031 (2023)
31. Z. Berktaş, E. Orhan, M. Ulusoy, M. Yildiz, S. Altındal, ACS Appl. Electron. Mater. **5**, 1804–1811 (2023)
32. E.H. Nicollian, A. Goetzberger, Bell Syst. Tech. J. **46**, 1055–1133 (1967)
33. A. Kaymaz, H. Uslu Tecimer, E. Evcin Baydilli, Ş. Altındal, J. Mater. Sci. Mater. Electron. **31**, 8349–8358 (2020)
34. V. Singh, N. Shashank, D. Kumar, R. Nahar, Radiat. Eff. Defects Solids. **166**, 80–88 (2011)

35. C.-H. Lin, E.J. Katz, J. Qiu, Z. Zhang, U.K. Mishra, L. Cao, L.J. Brillson, Appl. Phys. Lett. **103**, 162106 (2013)
36. S.M. Sze, K.N. Kwok, *Physics of Semiconductor Devices*, 3rd edn. (Wiley, New Jersey, 2007)
37. C. Nasr, S. Hotchandani, R.M. Leblanc, Proc. Indian Acad. Sci. **107**, 699–708 (1996)
38. A. Tataroglu, A. Buyukbas Ulusan, Ş Altındal, Y. Azizian Kalandaragh, J. Inorg. Organomet. Polym. Mater. **31**, 1668–1675 (2021)
39. N. Shiwakoti, A. Bobby, K. Asokan, B. Antony, Microelectron. Reliab. **69**, 40–46 (2017)
40. N.D. Reynolds, C.D. Panda, J.M. Essick, Am. J. Phys. **82**, 196–205 (2014)
41. D. Akay, U. Gokmen, S.B. Ocak, Phys. Scr. **94**, 115302 (2019)
42. R. Lok, E. Budak, E. Yılmaz, Microelectron. Reliab. **109**, 113663 (2020)
43. D.A. Oeba, J.O. Bodunrin, S.J. Moloi, Physica B **610**, 412786 (2021)
44. B. Akın, M. Ulusoy, S. Altındal, Yeriskin, Mater. Sci. Semicond. Process. **170**, 107951 (2024)
45. D. Akay, E. Seven, U. Gökmen, S. Bilge Ocak, ACS Appl. Nano Mater. **6**, 17482–17490 (2023)
46. M. Ulusoy, S. Altındal, P. Durmus, S. Ozcelik, Y. Azizian-Kalandaragh, J. Mater. Sci. Mater. Electron **32**, 13693–13707 (2021)


**Publisher's Note** Springer Nature remains neutral with regard to jurisdictional claims in published maps and institutional affiliations.